Electrical Impedance Tomography*

Margaret Cheney[†]
David Isaacson[†]
Jonathan C. Newell[†]

Abstract. This paper surveys some of the work our group has done in electrical impedance tomography.

1. Introduction. There are a variety of medical problems for which it would be useful to know the time-varying distribution of electrical properties inside the body.

By "electrical properties," we mean specifically the electric conductivity and permittivity. The electric conductivity is a measure of the ease with which a material conducts electricity; the electric permittivity is a measure of how readily the charges within a material separate under an imposed electric field. High-conductivity materials allow the passage of both direct and alternating currents; high-permittivity materials allow the passage of only alternating currents. Both of these properties are of interest in medical applications, because different tissues have different conductivities and permittivities.

One medical problem for which knowledge of internal electrical properties would be useful is the detection of pulmonary emboli, or blood clots in the lungs. The development of pulmonary emboli is a common, and often serious, complication of surgery. Unfortunately, at present the diagnosis is rather involved, requiring inhalation of radioactive gas in order to determine the ventilated lung region. This is followed by injection of a radio-opaque dye or a dissolved radioactive substance into a vein to make an image of the blood circulation. The image of the circulation in the lung is compared with the image of the ventilated region; areas that are ventilated but not perfused by blood indicate the presence of emboli.

However, another way to determine the location of gas and blood within the body would be to map the internal electric conductivity and permittivity. These electrical properties are very different for air, tissue, and blood; moreover, they vary on different time scales. Thus a time-varying map of the electrical properties should show lung regions that are ventilated but not perfused by blood.

Furthermore, determining the presence of pulmonary emboli from a map of the electrical properties would have a number of advantages over present techniques. It would require no exposure to X-rays or radioactive material. It could be done at the bedside, with a relatively small and inexpensive electrical system.

Information about the internal electrical properties of a body could have many other medical uses. Such information could potentially be used for the following [H]: monitoring for lung problems such as accumulating fluid or a collapsed lung, noninvasive monitoring of heart function and blood flow, monitoring for internal bleeding, screening for breast cancer, studying emptying of the stomach, studying pelvic fluid accumulation as a possible cause of pelvic pain, quantifying severity of premenstrual syndrome by determing the amount of intracellular vs. extracellular fluid, determining the boundary between dead and living tissue, measuring local internal temperature increases associated with hyperthermia treatments, and improving electrocardiograms [CF] and electroencephalograms.

A variety of nonclinical applications of electrical impedance tomography is also possible. These include imaging multiphase fluid flow [XHHB, WB], determining the location of mineral deposits in the earth [DL, P, SSS], tracing the spread of contaminants in the earth [RDLOC, RDBLR, DR], nondestructive evaluation of machine parts [ESIC], and control of industrial processes such as curing and cooking.

In order to map the electric conductivity and permittivity inside the body, our group at Rensselaer has designed and built an electronic system that applies currents through electrodes attached to the surface of the body and measures the resulting voltages. This system uses these electrical measurements to reconstruct and display approximate pictures of the electric conductivity and permittivity inside the body. This process is called electrical impedance tomography (EIT). The term "impedance" comes from circuit theory: it is the ratio of the voltage across a circuit element to the current through the element.

Below we describe the mathematical model for EIT. We use this model to describe some of the theory that gave rise to the design of the Rensselaer system, which we call the adaptive current tomography (ACT) system. Then we survey some reconstruction algorithms, focusing on the one that was used to make the images accompanying this paper.

2. The Mathematical Model. The electric potential u in the body Ω is governed by the equation

$$(2.1) \qquad \nabla \cdot \gamma(x, \omega) \nabla u = 0.$$

Here x is a point in Ω, u is the electric potential or voltage, and the admittivity γ is given by $\gamma(x, \omega) = \sigma(x, \omega) + i\omega\epsilon(x, \omega)$, where σ is the electric conductivity, ϵ is the electric permittivity, and ω is the angular frequency of the applied current. It is the admittivity of a block of homogeneous material that is proportional to the reciprocal of its impedance. Appendix 1 shows how (2.1) can be obtained from Maxwell's equations.

In practice, we apply currents to electrodes on the surface $\partial\Omega$ of the body. These currents produce a current density on the surface whose inward pointing normal component is denoted by j. Thus

$$(2.2) \qquad \gamma \frac{\partial u}{\partial \nu} = j \;\; \text{on} \;\; \partial\Omega.$$

One possible model for EIT is (2.1) and (2.2), together with the conservation of charge condition $\int_{\partial\Omega} j = 0$ and the condition $\int_{\partial\Omega} u = 0$, which amounts to choosing a "ground" or reference voltage. This model is the commonly used *continuum model*.

For the continuum model, we define the operator R by $Rj = v$, where v denotes the restriction of u to the boundary.

Unfortunately, the continuum model is a poor model for real experiments [CING], because we do not know the current density j. In practice, we know only the currents that are sent down wires attached to discrete electrodes, which in turn are attached to the body. One might approximate the unknown current density as a constant over each electrode (the *gap model*), but this model also turns out to be inadequate [CING].

We need to account for two main effects: the discreteness of the electrodes, and the extra conductive material (the electrodes themselves) we have added. We can do this as follows [CING, SCI].

The integral of the current density over the electrode is equal to the total current that flows to that electrode. Thus we have

$$(2.3) \qquad \int_{e_l} \gamma \frac{\partial u}{\partial \nu} ds = I_l, \qquad l = 1, 2, \ldots, L,$$

where I_l is the current sent to the lth electrode and e_l denotes the part of $\partial\Omega$ that corresponds to the lth electrode. This is combined with

$$(2.4) \qquad \gamma \frac{\partial u}{\partial \nu} = 0 \qquad \text{in the gaps between electrodes.}$$

The conventional way to model the very high conductivity of the electrodes is to impose the constraint that u is constant on each one. These constants, which we denote by V_l, are the voltages we measure. We write these constraints as

$$(2.5) \qquad u = \text{``}V_l\text{''} \quad \text{on} \ e_l, \qquad l = 1, 2, \ldots, L,$$

where the quotes are used to remind us that the V_l are not specified in advance but are part of the solution of the forward problem. This model we call the *shunt model*.

The shunt model, unfortunately, doesn't give results that agree with experimental data either [CING]. It fails to account for an electrochemical effect that takes place at the contact between the electrode and the body. This effect is the formation of a thin, highly resistive layer between the electrode and the body. The impedance of this layer is characterized by a number z_l, which we call the effective contact impedance or surface impedance. We therefore replace constraint (2.5) by

$$(2.6) \qquad u + z_l \gamma \frac{\partial u}{\partial \nu} = \text{``}V_l\text{''} \quad \text{on} \ e_l, \quad l = 1, 2, 3, \ldots, L.$$

The resulting model we call the *complete model*.

The complete model consists of (2.1), (2.2), (2.3), (2.4), and (2.6), together with the conditions

$$(2.7) \qquad \sum_{l=1}^{L} I_l = 0 \qquad \text{(conservation of charge)}$$

and

$$(2.8) \qquad \sum_{l=1}^{L} V_l = 0 \qquad \text{(choice of a ground)}.$$

This model has been shown to have a unique solution [SCI]. It is able to predict the experimental measurements to better than .1%.

3. Some Issues of System Design. At present, there is only one commercial EIT system. This is the applied potential tomography (APT) system invented by David Barber and Brian Brown [BB]. This system uses a single current source and 16 electrodes to make low-resolution images of conductivity changes inside the body.

One way to improve this system would be to improve its resolution. How can this be done? Certainly better resolution must involve using more electrodes. To study this idea, we introduce a quantitative measure of the ability of a current density j to distinguish two different admittivities γ and τ. Distinguishing between them means that the voltage difference $\|R(\gamma)j - R(\tau)j\|_\infty$ is greater than our measurement precision. (Here $\|\cdot\|_\infty$ denotes the supremum.) However, this voltage difference can be made arbitrarily large by applying a sufficiently high current. Since it is not practical or safe to apply all the power in the universe, we need some constraint.

What constraint is appropriate? Researchers have variously constrained the maximum magnitude of the currents [CI], the sum of the currents [EP, KE, KVKK], and the power [CI]. The present safety regulations [AAMI] constrain the sum of the currents. However, if a current of a given magnitude is applied to a sufficiently small electrode, the current density can become so high as to cause pain. These regulations are thus not appropriate, and are therefore being reexamined.

For medical applications, there are two physiological effects to consider. At low frequencies, nerves and muscles can respond to electric currents. At high frequencies, organs are subject to damage by heating. We believe that both safety concerns can be addressed by constraining the applied current density, which bounds the applied power as well.

Accordingly, we define [I] the "distinguishability" δ of γ from τ by a current density j to be

$$(3.1) \qquad\qquad \delta(j) = \frac{\|R(\gamma)j - R(\tau)j\|}{\|j\|},$$

where $R(\gamma)j$ denotes the electric potential or voltage on $\partial\Omega$ resulting from the application of the current density j to a body containing the admittivity distribution γ. Here, for simplicity, we use the $L^2(\partial\Omega)$ norm. A discussion of other norms can be found in [CI].

It was shown in [GIN2] that as the area of $\partial\Omega$ on which current is applied shrinks to zero, the distinguishability also goes to zero. In particular, if one increases the number of electrodes while applying current only between a pair of them, the distinguishability decreases.

This suggests that in order to improve resolution by increasing the number of electrodes, one should apply current to all the electrodes. It is for this reason that the Rensselaer ACT system has as many current generators as electrodes [GIN1].

A similar result [GIN2] also implies that EIT systems should use large electrodes that fill as much of $\partial\Omega$ as possible.

For a many-electrode, multiple-current-generator system, the question arises of which current density patterns should be used in order to best distinguish between two admittivity distributions γ and τ.

We say that the current density j is a "best" pattern for distinguishing γ from τ if j maximizes the distinguishability δ. Many readers will recognize (3.1) as the Rayleigh–Ritz quotient; it achieves its maximum when j is the eigenfunction of $|R(\gamma) - R(\tau)|$ corresponding to the largest eigenvalue.

As a simple example [GIN1], consider the problem of distinguishing a homogeneous annulus from a homogeneous disk with the same conductivity. In this case,

the eigenfunctions of $|R(\gamma) - R(\tau)|$ are trigonometric functions and the best current density is therefore simply $j(\theta) = \cos(\theta - \theta_0)$ for any θ_0. This example can be used to determine the size of the smallest object detectable in the center of an otherwise homogeneous medium by measurements of a given precision. We study the center because objects placed there have the least effect on boundary measurements.

In particular, [GIN1] calculated the size of the smallest centered cylindrical insulator (or conductor) whose presence can be detected in a homogeneous cylindrical tank with roughly the same diameter and conductivity as a human chest, when probed by a 32-electrode system with .1% accuracy. The results of these calculations agree with the experiments [CING, GIN1]. In particular, they show that a single current applied between an adjacent pair of electrodes cannot distinguish objects smaller than fist size in the center of a chest-sized tank. A single current applied between diametrically opposed electrodes cannot detect objects smaller than two fingers in diameter, while the "best" cosine pattern can detect an object the diameter of a single finger in the center of a chest-sized tank.

If the conductivity σ is not rotationally invariant, then the cosine is not necessarily the best current density to distinguish σ from a homogeneous conductivity τ. In general, since the best current densities depend on the unknown conductivity σ inside the body, they cannot be known in advance. They can be determined, however, by the adaptive process described in Appendix 2.

The alert reader may be wondering at this point why we pay so much attention to best current densities. After all, the mathematical model is linear, so on a system with a limited number of electrodes, we should be able to apply any linearly independent set of current patterns, and from the corresponding measured voltages, synthesize the result of applying any other current pattern.

The problem is that the measurement process introduces nonlinearities. For example, a nonzero voltage that is smaller than the measurement precision of the voltmeter will register as zero. In other words, the measurement process causes information to be lost. An adaptive measurement scheme for obtaining the most possible information is discussed in Appendix 2.

How many current patterns should we apply? Although in theory, we would need to apply all possible current patterns in order to obtain all possible information, in practice this would take too much time. Because the problem is very close to being linear, we apply only a linearly independent set of patterns that are chosen to have maximal information content (in the sense of being the best for distinguishing the medium from a homogeneous guess).

4. Reconstruction Algorithms. The reconstruction problem is to obtain an approximation to γ in the interior from the boundary measurements. This problem is challenging because it is not only nonlinear, but also ill posed, which means that large changes in the interior can correspond to very small changes in the measured data.

From a theoretical point of view, all possible boundary measurements do uniquely determine the admittivity in the interior [KV, SU, N]. However, in practice we are limited to a finite number of electrodes and a finite number of current patterns.

Many reconstruction algorithms have been proposed. We outline several of the different approaches and then describe in more detail the methods we used to make the images that accompany this paper.

The different approaches fall into several categories. The first are based on linear approximations. These are noniterative methods based on the assumption that the

conductivity does not differ very much from a constant. Examples of linear methods are the Barber–Brown backprojection method [BB] and related methods [SV, BT], Calderón's approach [C, IC2, II, CII, IC], moment methods [BAG, CW, AS], and one-step Newton methods [CINGS, B, ESIC, FCIGN, G, S]. The images in this paper were made with a one-step Newton method that is close to being an approximate linearization; this we discuss in more detail below.

Another class of methods is iterative methods. These include, typically, output least squares for various functionals. Examples include [ESIC, KM, WFN, YWT, JIEN, H, WWT, BP, J, D, K, SV]. The papers [D] and [K], in particular, contain rigorous proofs of convergence of Newton-type methods under various conditions.

A related class includes the adaptive methods, in which the applied patterns of current are adjusted to get the best reconstruction [GIN1, GIN2, NGI, S, BP, ICp].

One promising method is a layer-stripping algorithm [Sy, SCII]. It is based on the idea of first finding the electrical parameters on the boundary of the body, then mathematically stripping away this outermost known layer. Then the process is repeated, and the medium is stripped away, layer-by-layer, with the electrical parameters being found in the process. This method is appealing because it is fast, addresses the full nonlinear problem, and works well on continuum-model synthetic data. However, no available layer-stripping algorithm works well on complete-model data.

There are also more theoretical papers that present formulas or suggestions for reconstructions, implementations of which have not been published. Such papers are [SU, N, R, R2, C, IC2].

5. The Noser Algorithm and Its Implementation. For an L-electrode system, we apply a linearly independent set of current patterns. Because of the constraint (2.7), a full set contains $L-1$ current patterns, which we denote by $I^1, I^2, \ldots, I^{L-1}$, where $I^k = (I_1^k, I_2^k, \ldots, I_L^k)$. The corresponding voltage patterns we denote by V^1, $V^2, \ldots, V^{L-1}$. One might think that from voltages measured on L electrodes, for $L-1$ current patterns, we would have $L(L-1)$ independent degrees of freedom. However, by (2.8), the voltages are constrained by the choice of a reference voltage, so in fact we have only $L-1$ measurements for each current pattern. Moreover, some of this data is redundant, because the current-voltage map is symmetric. Thus the number of independent degrees of freedom is the number of degrees of freedom of a symmetric $(L-1) \times (L-1)$ matrix, namely, $L(L-1)/2$. For our ACT3 system, which has $L = 32$ electrodes, the number of degrees of freedom is 496.

For simplicity, we consider only the problem of reconstructing the conductivity σ, or, alternatively, the resistivity $\rho = 1/\sigma$. We can only hope to recover a limited number of degrees of freedom of ρ; we denote these degrees of freedom by $\rho_1, \rho_2, \ldots, \rho_N$, where $N \leq L(L-1)/2$. For example, ρ could be represented by specifying its averages over small mesh elements; the average over the nth mesh element would be denoted ρ_n. Henceforth we will assume that ρ is completely determined by the ρ_n. We would like to find a conductivity ρ whose voltage patterns $U^1(\rho), U^2(\rho), \ldots, U^{L-1}(\rho)$ are equal to the measured ones. To do this, we attempt to minimize the functional

$$(5.1) \qquad\qquad E(\rho) = \sum_{k=1}^{L-1} \|U^k(\rho) - V^k\|^2.$$

To minimize this functional, we differentiate with respect to each degree of freedom ρ_n, and set the derivatives to zero. This gives us the following set of N nonlinear

equations to solve:

$$(5.2) \qquad 0 = \frac{\partial E(\rho)}{\partial \rho_n} = 2 \sum_{k=1}^{L-1} (U^k(\rho) - V^k) \cdot \frac{\partial U^k(\rho)}{\partial \rho_n}.$$

A standard method for solving such a system of nonlinear equations is Newton's method; the NOSER code takes one step of a (regularized) Newton's method, from an initial guess of a uniform resistivity, and displays the result. The advantage of taking only one step is that the Jacobian matrix for the uniform case can be calculated ahead of time and stored. Thus the reconstruction is done via the formula (from [E])

$$(1) \qquad \rho = \rho^0 C + 2 \sum_{k=1}^{K} \sum_{j=1}^{K} v_{k,j} S^{k,j},$$

where C and $S^{k,j}$ are precomputed vectors of length 496 that depend only on known factors such as the geometry and regularization, and where ρ^0 and $v_{k,j}$ are scalars computed from inner products of the data with known vectors.

This algorithm was implemented on a 386 personal computer with an Alacron AL860 AT printed circuit board, which relies on the Intel i860 microprocessor. This board has a data retrieval rate of 160 Megabytes per second and is capable of 80 Megaflops maximum throughput. Our implementation of the above algorithm on this board achieves a rate of 60 reconstructions per second. More details about the implementation are given in [E].

6. Some Experimental Tests. Our present third generation system, ACT3, incorporates the fast algorithm of section 5 together with electronics that are designed according to the principles of section 2. This system is capable of making 20 images per second with data accurate to one part in 2^{15}, using a single array of 32 electrodes.

We have used this system to conduct many experiments, some of which are illustrated in the figures. We have done experiments in a test tank (Figures 1 and 2), on a human volunteer (Figures 3, 4, and 5), and on dogs (Figures 5 and 6).

The dog experiments are intended to test the feasibility of using electrical impedance tomography to detect pulmonary emboli. The dog was prepared so that the left and right lungs could be ventilated separately. Figure 6 shows the result of closing off the ventilation of one lung at a time. Then a balloon catheter was used to occlude a major branch of the pulmonary artery, to simulate a pulmonary embolus. Figure 7 shows the result.

7. Future Challenges. Many challenges still remain to be overcome before EIT will provide a clinically useful device. The challenges can be classified into the areas of electronics, algorithms, and clinical applications.

Because the problem is intrinsically so ill posed, the measurements must be made very accurately. For clinical applications, they must also be made fast. Finally, a great many electrodes should be used to obtain good images. In particular, because current does not confine itself to a plane, measurements should be made on as large a surface as possible, which means that many electrodes should be used.

The ill-posedness and nonlinearity of the reconstruction problem also make algorithm development difficult. The NOSER and the backprojection algorithms have the advantage of being fast, but they are not very accurate. Algorithms need to be developed that are fast and accurate and that apply to a wide range of surface geometries.
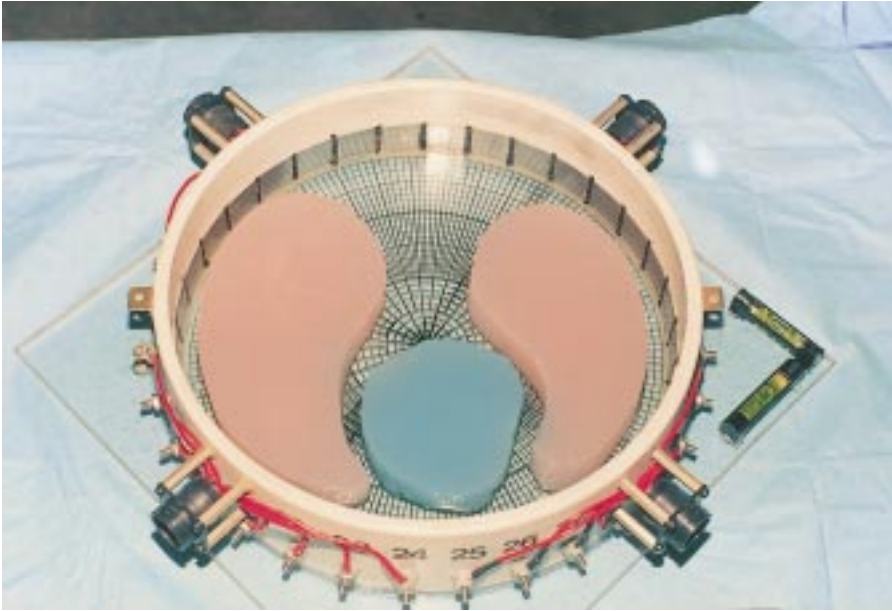
Fig. 1 *A test tank containing "lungs" and "heart" made of agar with varying amounts of added salt. This tank is filled with salt water, and used as a test body for the EIT system. Note the large electrodes around the inner circumference of the tank.*
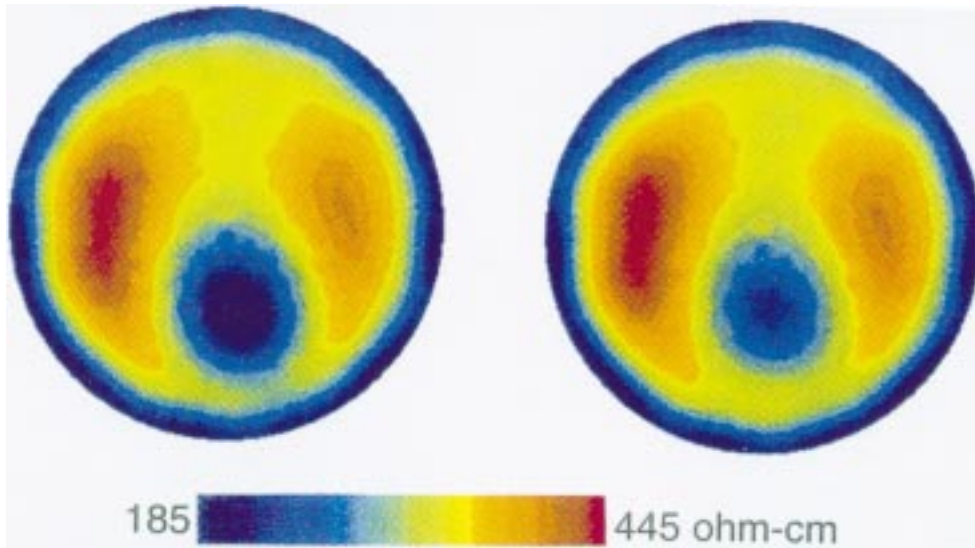

Fig. 2 *Images of the resistivity of two different test tanks like the one shown in Figure 1. The two different tanks had hearts of different sizes, meant to simulate different times during the heart's cycle.*

Finally, the ill-posedness of the problem also makes it unlikely that EIT images, even with many electrodes, will have resolution comparable to that of CT or MRI

Fig. 3 *The ACT 3 system with 32 electrodes encircling the chest of a subject. Here the goal is to make images that show the changes in volumes of air and blood that occur with breathing and the pulsatile circulation of the blood. Such images are referred to as ventilation and perfusion images, respectively. This is one possible positioning of electrodes for this purpose.*

images. However, EIT is low cost, noninvasive, and provides information about the electrical parameters of the body, which is information that cannot be obtained by these other methods. Specific clinical applications still need to be explored.

Appendix 1: Derivation of (2.1) from Maxwell's Equations. The fixed-frequency version of Maxwell's equations is
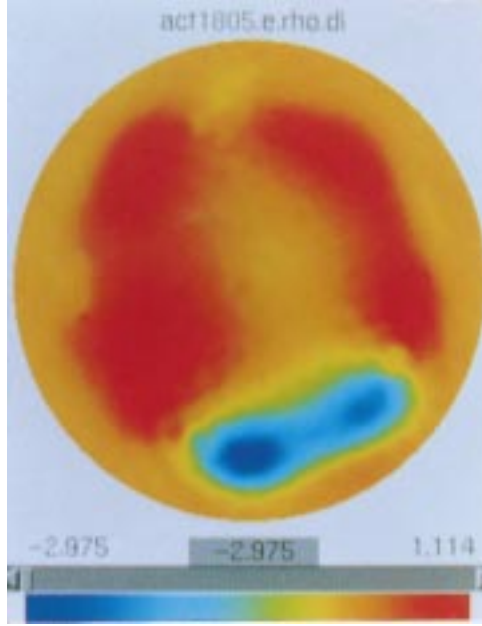
$$\nabla \wedge E = -i\omega\mu H, \tag{A.1}$$

Fig. 4 *This is a "perfusion" image of a human subject. It was produced with the electrodes configured as in Figure* 3. *This image is a difference image, formed by subtracting images taken at two different times. The first image was made when the heart's ventricles have contracted, and the second was made when the heart's ventricles are filled with blood. In this difference image, the lung region shows an increase in the magnitude of the admittivity, while the ventricles' region shows a decrease in admittivity. This is because blood (which has high admittivity) has traveled from the heart to the lungs.*

$$\nabla \wedge H = \sigma E + i\omega\epsilon E, \tag{A.2}$$

where E denotes the electric field, H denotes the magnetic field, and $\nabla\wedge$ denotes the curl operator. In order to determine whether our parameter ranges are such that we can find a simplifying approximation to these equations, we first write the equations in nondimensional form. To this end, we write $E = [E]\tilde{E}$, $H = [H]\tilde{H}$, $x = [x]\tilde{x}$, and $\nabla\wedge = [x]^{-1}\tilde{\nabla}\wedge$, where the quantities in brackets are scalars carrying the units, and the quantities with tildes are nondimensional vectors.

With this notation, we can write (A.1) and (A.2) as

$$\tilde{\nabla} \wedge \tilde{E} = -i\omega\mu\frac{[H][x]}{[E]}\tilde{H}, \tag{A.3}$$

$$\tilde{\nabla} \wedge \tilde{H} = \sigma\frac{[E][x]}{[H]}\tilde{E} + i\omega\epsilon\frac{[E][x]}{[H]}\tilde{E}. \tag{A.4}$$

If we now choose units for $[E]$ and $[H]$ so that $\sigma[E][x]/[H] = 1$, then we can write (A.3) and (A.4) as

$$\tilde{\nabla} \wedge \tilde{E} = -i\omega\mu\sigma[x]^2\tilde{H}, \tag{A.5}$$

$$\tilde{\nabla} \wedge \tilde{H} = \tilde{E} + i\frac{\omega\epsilon}{\sigma}\tilde{E}. \tag{A.6}$$
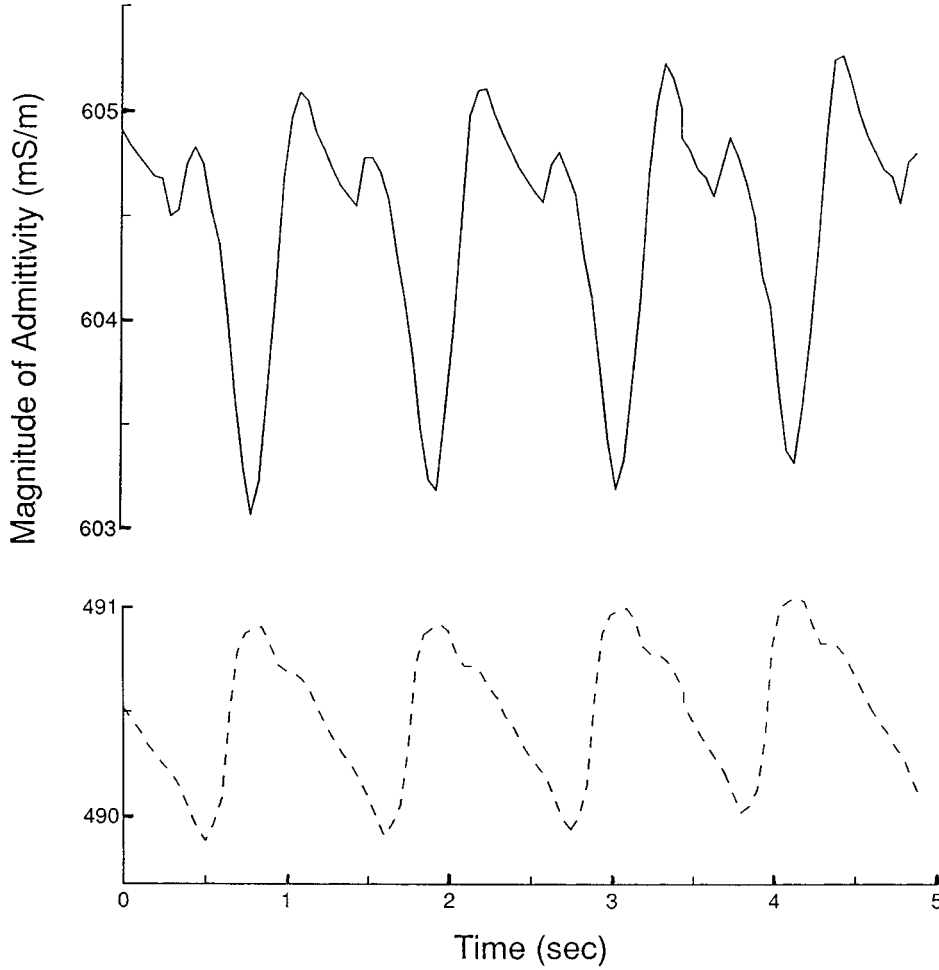
Fig. 5 *These graphs illustrate the periodic filling and emptying of the heart (top) and lungs (bottom). The top curve is an average of the magnitude of the admittivity over one of the ventricular regions shown in Figure 4, plotted against time. The bottom curve is an average of admittivity of the lung region shown in Figure 4, plotted against time. Note that the admittivity of the ventricular region decreases rapidly when the ventricles contract and pump highly conductive blood out to the body, while simultaneously the lungs' admittivity increases rapidly as they fill with blood.*

Electrical impedance tomography systems operate in the range where $\omega\mu\sigma[x]^2$ is negligible. The ACT3 system, for example, operates at 28.8 kHz, and is applied to bodies smaller than 1 meter in which the conductivity is generally less than 1 (Ohm-meter)$^{-1}$. The system of [ESIC], although used to examine metals of high conductivity, operated at a very low frequency.

If the right side of (A.5) is negligible, then we can neglect the right side of (A.1) to conclude that E is the gradient of a potential. In particular, we write

$$(A.7) \qquad\qquad\qquad E = -\nabla u,$$

where u is the electric potential. Using (A.7) in the equation obtained by taking the divergence of (A.2), we obtain (2.1).
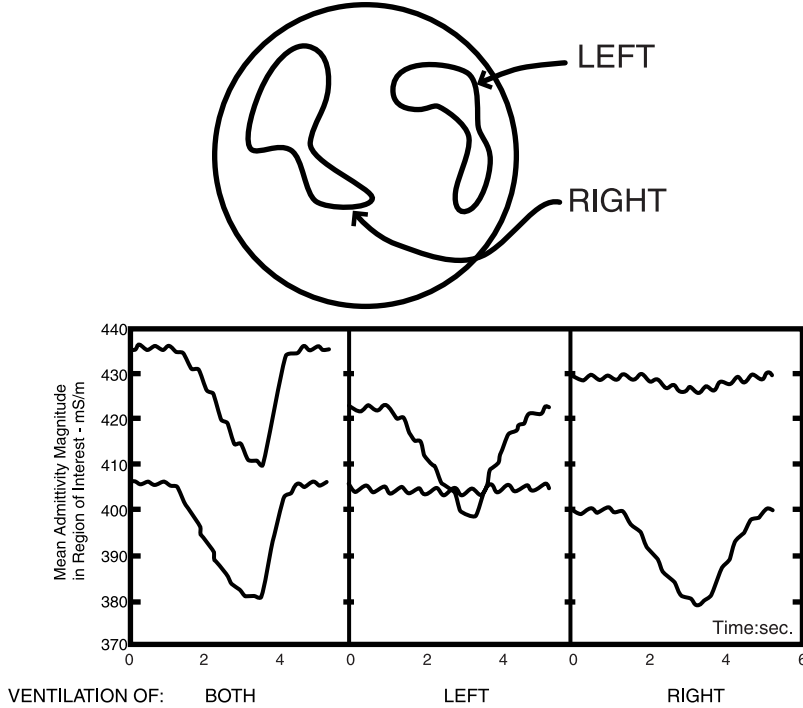
Fig. 6 *Mean admittivity magnitude in the two regions of interest shown in the diagram at the top is shown versus time in the three panels at the bottom. In the first panel, a breath with a tidal volume of 300 ml/side was administered to BOTH lungs. In the middle panel, a 300 ml breath was applied to only the LEFT lung; in the third panel, the breath was applied to only the RIGHT lung. The curves in each panel show the admittivity magnitude in the region of the left chest at the top of each panel, and in the right chest at the bottom of each panel. The area of the left and right regions of interest was 7.9% and 12.1% of the total image area, respectively. The boundaries of these regions are iso-admittivity contours selected in an image of bilateral ventilation.*

To obtain (2.2), we must consider also a current applied to the surface of the body. Thus (A.2) is modified as

$$(A.8) \qquad\qquad \nabla \wedge H = J^{appl} + \gamma E.$$

Taking the divergence of (A.8) and using (A.7) gives us

$$(A.9) \qquad\qquad \nabla \cdot \gamma \nabla u = \nabla \cdot J^{appl}.$$

We integrate both sides of (A.9) over a pillbox Ω_δ of thickness δ enclosing part of the boundary, and use the divergence theorem. In the limit as the thickness δ goes to zero, we find

$$(A.10) \qquad\qquad \gamma_{out}\partial_\nu u - \gamma_{in}\partial_\nu u = \nu \cdot J^{appl}_{out} - \nu \cdot J^{appl}_{in},$$

where ν denotes the outer unit normal vector. We assume that γ outside the body is negligible, so the first term on the left side of (A.10) vanishes. We also assume that the current J^{appl} is applied only on the outer surface of the body, so that J^{appl}_{in} is
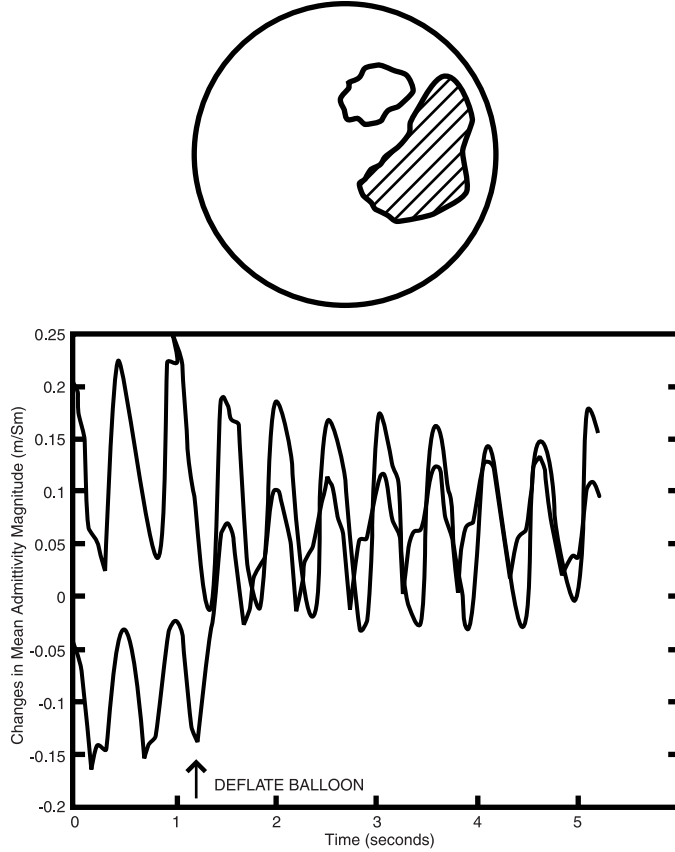
Fig. 7 *Change in mean admittivity magnitude in two regions of interest with deflation of a balloon located in a branch of the pulmonary artery. The regions of interest are shown at top, and are contours of iso-admittivity. The reference admittivity of each curve is different, and has been subtracted to allow both curves to be displayed on the same axes.*

zero. We define $j = -\nu \cdot J^{appl}$, so that j denotes the applied current entering the body. This gives us (2.2).

Careful computations [Doer] show that for the operating parameters of the Rensselaer ACT3 system, modeling error is about fifteen hundredths of a percent. The electronics of ACT3 are accurate to about three hundredths of a percent. This is accurate enough to detect the modeling error, which implies that the images might be improved by using the full Maxwell's equations.

Appendix 2: Adaptive Process for Finding Best Patterns. In order to find the best single-current density for distinguishing γ from τ, we can use the following adaptive process [Ip, IC].

1) Guess any current density j_0 for which $\int_{\partial\Omega} j_0 = 0$ and $\|j_0\| = 1$. Set $k = 0$.

2) Measure the voltage on $\delta\Omega$:

$$V_k^1 = R(\tau)j_k.$$

3) Compute the voltage on $\partial\Omega$:

$$V_k^0 = R(\gamma)j_k.$$

4) Compute the new estimate j_{k+1} to the best current density by

$$j_{k+1} = \frac{V_k^1 - V_k^0}{\|V_k^1 - V_k^0\|}.$$

5) If the change in j is less than the measurement precision ϵ, i.e.,

$$\|j_{k+1} - j_k\| < \epsilon,$$

stop; otherwise increment k and repeat, starting with step 2.

This algorithm is essentially the power method for finding the largest eigenvalue and corresponding eigenvector of a matrix [IK].

Numerical and experimental tests of this adaptive process by 32-electrode ACT systems [NGI, GIN1, ESIC] have shown as much as a 30-fold improvement in distinguishability within 5 iterations.

Now, suppose we wish not merely to determine whether γ is distinguishable from τ, but to obtain all possible information that will enable us to distinguish between the two, perhaps for the purpose of forming an image of the difference $\gamma - \tau$. We could do this by using the above algorithm to find the best pattern, then searching the orthogonal complement for the next best pattern, etc. Alternatively, we can find all the best patterns at once by the following procedure.

We denote by $\Re$ the boundary map for the complete model, i.e., $\Re I = V$, where I and V are now L-dimensional vectors of currents and voltages. We denote by $\delta\Re$ the difference map $\Re(\gamma) - \Re(\tau)$. We want to determine the eigenvectors of $\delta\Re$, without knowing τ in advance.

Suppose we first apply any orthonormal set $\{T^l, l = 1, 2, \ldots, L - 1\}$ of current patterns, and denote the corresponding voltage patterns by $\{(\delta\Re)T^l, l = 1, 2, \ldots, L - 1\}$.

We wish to find vectors I such that

(A2.1) $(\delta\Re)I = \rho I,$

where the eigenvalue ρ is a scalar. We assume that we can write I as a linear combination of the T's:

(A2.2) $I = \sum_{l=1}^{L-1} q_l T^l;$

we need only determine the q's. On both sides of (A2.1) we use the expression (A2.2) for I, thus obtaining

(A2.3) $\sum_{l=1}^{L-1} q_l (\delta\Re)T^l = \rho \sum_{l=1}^{L-1} q_l T^l.$

We now take the inner product of (A2.3) with the vector T^k, using the orthonormality of the T's. This results in

(A2.4) $\sum_{l=1}^{L-1} q_l \langle T^k, (\delta\Re)T^l \rangle = \rho q_k,$

where we have used $\langle \cdot, \cdot \rangle$ to denote the inner product. Equation (A2.4) tells us that the desired q's are the eigenvectors of the matrix whose elements are $\langle T^k, (\delta\Re)T^l \rangle$; this matrix, moreover, is one that we can compute from experimental measurements!

The subtle point is that this process must be iterated. This is because the operator $\delta\Re$ is not known exactly; our knowledge of it depends on the current patterns we apply.

REFERENCES

[AAMI]   *Safe Current Limits for Electromedical Apparatus*, ANSI/AAMI ES 1-1993. Copies are available from the Association for the Advancement of Medical Instrumentation, 3330 Washington Boulevard, Suite 400, Arlington, VA 22201–4598.

[AS]   A. ALLERS AND F. SANTOSA, *Stability and resolution analysis of a linearized problem in electrical impedance tomography*, Inverse Problems, 7 (1991), pp. 515–533.

[B]   R.S. BLUE, *A real-time three-dimensional linearized reconstruction algorithm generalized for multiple planes of electrodes*, Ph.D. Thesis, Rensselaer Polytechnic Institute, Troy, NY, 1997.

[BP]   W.R. BRECKON AND M.K. PIDCOCK, *Some mathematical aspects of electrical impedance tomography*, in Mathematics and Computer Science in Medical Imaging, M.A. Viergever and A.E. Todd-Pokropek, eds., NATO ASI Series, F39, Springer-Verlag, New York, 1988 pp. 351–362; also *Progress in electrical impedance tomography*, in Some Topics on Inverse Problems, P.C. Sabatier, ed., World Scientific, River Edge, NJ, 1988, pp. 254–264.

[BT]   C. BERENSTEIN AND E.C. TARABUSI, *Inversion formulas for the k-dimensional Radon transform in real hyperbolic spaces*, Duke Math. J., 62 (1991), pp. 1–19.

[BAG]   S. BERNTSEN, J.B. ANDERSEN, AND E. GROSS, *A General Formulation of Applied Potential Tomography*, preprint.

[BB]   D.C. BARBER AND B.H. BROWN, *Applied potential tomography*, J. Phys. E. Sci. Instrum., 17 (1984), pp. 723–733.

[BBS]   B. H. BROWN, D. C. BARBER, AND A. D. SEAGAR, *Applied potential tomography: Possible clinical applications*, Clin. Phys. Physiol. Meas., 6 (1985), pp. 109–121.

[C]   A.P. CALDERÓN, *On an inverse boundary value problem*, Seminar on Numerical Analysis and Its Applications to Continuum Physics, Soc. Brasileira de Matemàtica, Rio de Janeiro, 1980, pp. 65–73.

[CF]   P. COLLI FRANZONE, *Il probleme inverso dell'elettrocardiografia*, Boll. Un. Mat. Ital. A, 15 (1978), pp. 30–51; and P. Colli Franzone, L. Guerri, B. Taccardi, and C. Viganotti, *The Direct and Inverse Potential Problems in Electrodcardiology. Numerical Aspects of Some Regularization Methods and Application to Data Collected in Isolated Dog Heart Experiments*, Pub. 222, Laboratorio di Analisi Numerica del Consiglio Nazionale delle Ricerche, Pavia, Italy, 1979.

[CI]   M. CHENEY AND D. ISAACSON, *Distinguishability in impedance imaging*, IEEE Trans. Biomed. Engr., 39 (1992), pp. 852–860.

[CI2]   M. CHENEY AND D. ISAACSON, *An overview of inversion algorithms for impedance imaging*, in Inverse Scattering and Applications, O. H. Sattinger, C. A. Tracy, and S. Venakides, eds., AMS, Providence, RI, 1991.

[CII]   M. CHENEY, D. ISAACSON, AND E.L. ISAACSON, *Exact solutions to a linearized inverse boundary value problem*, Inverse Problems, 6 (1990), pp. 923–934.

[CING]   K.-S. CHENG, D. ISAACSON, J. C. NEWELL, AND D. G. GISSER, *Electrode models for electric current computed tomography*, IEEE Trans. Biomed Engr., 36 (1989), pp. 918–924.

[CINGS]   M. CHENEY, D. ISAACSON, J. NEWELL, J. GOBLE, AND S. SIMSKE, *NOSER: An algorithm for solving the inverse conductivity problem*, Internat. J. Imaging Systems and Technology, 2 (1990), pp. 66–75.

[CW]   T.J. CONNOLLY AND D.J.N. WALL, *On an inverse problem, with boundary measurements, for the steady state diffusion equation*, Inverse Problems, 4 (1988), pp. 995–1012.

[D]   D.C. DOBSON, *Convergence of a reconstruction method for the inverse conductivity problem*, SIAM J. Appl. Math., 52 (1992), pp. 442–458.

[DL]   K.A. DINES AND R.J. LYTLE, *Analysis of electrical conductivity imaging*, Geophysics, 46 (1981), pp. 1025–1036.

[DR]   W. DAILY AND A. RAMIREZ, *Electrical resistance tomography during in-situ tricholoethylene remediation at the Savannah River Site*, Applied Geophysics, 33 (1995), pp. 239–249.

[Doer] B. DOERSTLING, *A 3-D Reconstruction Algorithm for the Linearized Inverse Boundary Value Problem for Maxwell's Equations*, Ph.D. Thesis, Rensselaer Polytechnic Institute, Troy, NY, 1995.

[E]   P. EDIC, *The Implementation of a Real-Time Electrical Impedance Tomograph*, Ph.D. Thesis, Rensselaer Polytechnic Institute, Troy, NY, 1994.

[EP]   B. M. EYÜBOGLU AND T.C. PILKINGTON, *Comments on distinguishability in electrical impedance tomography*, IEEE Trans. Biomed. Engr., 40 (1993), pp. 1328–1880.

[ESIC] M.R. EGGLESTON, R.J. SCHWABE, D. ISAACSON, AND L.F. COFFIN, *The application of electric current computed tomography to defect imaging in metals*, in Review of Progress in Quantitative NDE, D.O. Thompson and D.E. Chimenti, eds., Plenum, New York, 1989.

[FCIGN] L.F. FUKS, M. CHENEY, D. ISAACSON, D.G. GISSER, AND J.C. NEWELL, *Detection and imaging of electric conductivity and permittivity at low frequency*, IEEE Trans. Biomed. Engr., 3 (1991), pp. 1106–1110.

[G]   J.C. GOBLE, *The Three-Dimensional Inverse Problem in Electric Current Computed Tomography*, Ph.D. Thesis, Rensselaer Polytechnic Institute, Troy, NY, 1990.

[GB]   L.E. BAKER AND L.A. GEDDES, *Principles of Applied Biomedical Instrumentation*, 3rd ed., Wiley, New York, 1989.

[GIN1] D.G. GISSER, D. ISAACSON, AND J.C. NEWELL, *Theory and performance of an adaptive current tomography system*, Clin. Phys. Physiol. Meas. 9, Suppl. A (1988), pp. 35–41.

[GIN2] D.G. GISSER, D. ISAACSON, AND J.C. NEWELL, *Electric current computed tomography and eigenvalues*, SIAM J. Appl. Math., 50 (1990), pp. 1623–1634.

[GIN3] D.G. GISSER, D. ISAACSON, AND J.C. NEWELL, *Current topics in impedance imaging*, Clin. Phys. Physiol. Meas., 8A (1987), pp. 39–46.

[H]   D. HOLDER, *Clinical and physiological applications of electrical impedance tomography*, UCL Press, London, 1993.

[I]   D. ISAACSON, *Distinguishability of conductivities by electric current computed tomography*, IEEE Trans. Med. Imaging, MI-5 (1986), pp. 91–95.

[IC]   D. ISAACSON AND M. CHENEY, *Current problems in impedance imaging*, in Inverse Problems in Partial Differential Equations, D. Colton, R. Ewing, and W. Rundell, eds., SIAM, Philadelphia, 1990, pp. 141–149.

[IC2]   D. ISAACSON AND M. CHENEY, *Effects of measurement precision and finite numbers of electrodes on linear impedance imaging algorithms*, SIAM J. Appl. Math., 51 (1991), pp. 1705–1731.

[ICp]   D. ISAACSON AND M. CHENEY, *Process for Producing Optimal Current Patterns for Electrical Impedance Tomography*, U.S. Patent 5,588,429; Dec. 31, 1996.

[II]   D. ISAACSON AND E. ISAACSON, *Comment on Calderón's paper: 'On an inverse boundary value problem'*, Math. Comp., 52 (1989), pp. 553–559.

[IK]   E. ISAACSON AND H. B. KELLER, *Analysis of Numerical Methods*, Wiley, New York, 1966.

[Ip]   D. ISAACSON, *Process and Apparatus for Distinguishing Conductivities by Electric Current Computed Tomography*, U.S. Patent 4,920,490; April 24, 1990.

[J]   X. JIANG, *Augmented Lagrangian Method for Reconstructing Conductivity by Boundary Measurements*, Research summary, preprint.

[JIEN] H. JAIN, D. ISAACSON, P. M. EDIC, AND J. C. NEWELL, *Electrical impedance tomography of complex conductivity distributions with noncircular boundary*, IEEE Trans. Biomed. Engr., 44 (1997), pp. 1051–1060.

[K]   M. KLIBANOV, *Newton-Kantorovich Method for Impedance Computed Tomography*, preprint.

[KE]   A. KOSKAL AND B.M. EYÜBOGLU, *Determination of optimum injected current patterns in electrical impedance tomography*, Physiol. Meas., 16 (1995), pp. A99–A109.

[KVKK] V. KOLEHMAINEN, M. VAUHKONEN, P.A. KARJALAINEN, AND J.P. KAIPIO, *Assessment of errors in static electrical impedance tomography with adjacent and trigonometric current patterns*, Physiol. Meas., 18 (1997), pp. 289–303.

[KM]   R.V. Kohn and A. McKenney, *Numerical implementation of a variational method for electrical impedance imaging*, Inverse Problems, 9 (1990), pp. 389–414.

[KV]   R. Kohn and M. Vogelius, *Determining conductivity by boundary measurements*, Comm. Pure Appl. Math., 37 (1984), pp. 113–123.

[N]   A.I. Nachman, *Reconstruction from boundary measurements*, Ann. of Math., 128 (1988), pp. 531–576.

[N2]   A.I. Nachman, *Global uniqueness for a two-dimensional inverse boundary value problem*, Ann. of Math., 143 (1996), pp. 71–96.

[NGI]   J.C. Newell, D.G. Gisser, and D. Isaacson, *An electric current tomograph*, IEEE Trans. Biomed. Engr., 35 (1988), pp. 828–833.

[P]   R.L. Parker, *The inverse problem of resistivity sounding*, Geophysics, 42 (1984), pp. 2143–2158.

[R]   A. G. Ramm, *Multidimensional inverse scattering problems and completeness of the products of solutions to homogeneous PDE*, Z. Angew. Math. Mech., 69 (1989), pp. T13–T22.

[R2]   A. G. Ramm, *Finding conductivity from boundary measurements*, Comput. Math. Appl., 21 (1991), pp. 85–91.

[RDLOC]   A. Ramirez, W. Daily, D. LaBrecque, E. Owen, and D. Chesnut, *Monitoring an underground steam injection process using electrical resistance tomography*, Water Resources Research, 29 (1993), pp. 73–87.

[RDBLR]   A. Ramirez, W. Daily, A. Binley, D. LaBrecque, and D. Roelant, *Detection of leaks in underground storage tanks using electrical resistance methods*, J. Environmental and Engineering Geophysics, 1 (1996), pp. 189–203.

[S]   S. Simske, *An Adaptive Current Determination and a One-Step Reconstruction Technique for a Current Tomography System*, Master's Thesis, Rensselaer Polytechnic Institute, Troy, NY, 1987.

[Sy]   J. Sylvester, *A convergent layer stripping algorithm for radially symmetric impedance tomography problem*, Comm. Partial Differential Equations, 17 (1992), pp. 1955–1994.

[SCI]   E. Somersalo, M. Cheney, and D. Isaacson, *Existence and uniqueness for electrode models for electric current computed tomography*, SIAM J. Appl. Math., 52 (1992), pp. 1023–1040.

[SCII]   E. Somersalo, M. Cheney, D. Isaacson, and E.L. Isaacson, *Layer-stripping: A direct numerical method for impedance imaging*, Inverse Problems, 7 (1991), pp. 899–926.

[SSS]   S. Stphanesco, C. Schlumberger, and M. Schlumberger, *Sur la distribution électrique autour d'une prise de terre ponctuelle dans un terrain a couchés horizontales, homogènes et isotropes*, J. Physics & Radium Ser., 7 (1930), pp. 132–140.

[SU]   J. Sylvester and G. Uhlmann, *A uniqueness theorem for an inverse boundary value problem in electrical prospection*, Comm. Pure Appl. Math., 39 (1986), pp. 91–112; *A global uniqueness theorem for an inverse boundary value problem*, Ann. of Math., 125 (1987), pp. 153–169; *Inverse boundary value problems at the boundary—continuous dependence*, Comm. Pure Appl. Math., 41 (1988), pp. 197–221.

[SV]   F. Santosa and M. Vogelius, *A backprojection algorithm for electrical impedance imaging*, SIAM J. Appl. Math., 50 (1990), pp. 216–243.

[WB]   R.A. Williams and M.S. Beck, eds., *Process Tomography–Principles, Techniques and Applications*, Butterworth-Heinemann, Oxford, UK, 1995.

[WFN]   A. Wexler, B. Fry, and M.R. Neiman, *Impedance-computed tomography algorithm and system*, Appl. Opt., 24 (1985), pp. 3985–3992.

[WWT]   E.J. Woo, J. Webster, and W. J. Tompkins, *The improved Newton-Raphson method and its parallel implementation for static impedance imaging*, Proc. IEEE-EMBS Conf. Part 1, 5 (1990), pp. 102–103.

[XHHB]   C.G. Xie, S.M. Huang, B.S. Hoyle, and M.S. Beck, *Tomographic imaging of industrial process equipment–Development of system model and image reconstruction algorithm for capacitive tomography*, Sensors & Their Applications V, Edinburgh, Sept. 1991, pp. 203–208.

[YWT]   T.J. Yorkey, J.G. Webster, and W.J. Tompkins, *Comparing reconstruction algorithms for electrical impedance tomography*, IEEE Trans. Biomed. Engr., BME-34 (1987), pp. 843–852.